On the Plastic Deformation of a Tube During Bending

K. Pan*

K. A. Stelson

Department of Mechanical Engineering,
University of Minnesota,
111 Church Street,
Minneapolis, MN 55455

The objective of this study is to develop an analytical approach to calculate the relationship between the axial curvature of a bent tube and the resulting deformation of the cross-section. The model accounts for both geometrical and material nonlinearities. An approximate expression in trigonometric form is introduced for the displacement field, which reflects the change of wall thickness and neutral axis shift during bending. The total deformation theory is employed as a constitutive relation. The solution is found using a minimization approach and the energy principle. A better approach for springback prediction might be obtained from the deformation model, which predicts a more accurate moment of inertia change during bending.

Introduction

The ultimate goal of this study is to improve the precision of the real-time control for a tube bending system by predicting a more accurate springback angle. Tube bending is frequently required in many manufacturing industries. One disadvantage of the rotary-draw bending process is that a tube will spring back after it is unloaded due to the elastic property of the material. To achieve a desired bend angle, the tube must be overbent to compensate for the springback.

Traditionally springback compensation is accomplished using the operator's skill and experience. Several test bends are required before a correct springback compensation can be found. As a result, tube bending becomes a trial-and-error process.

On a rotary-draw bending machine, the springback of a tube has two sources: one is the spring back of the plastically curved part of the tube; the other is the spring back due to the elastic deformation in the pressure die area. The total springback is the sum of these two. In this paper, the former is studied.

The springback of the curved tube, θ_s, can be found by integrating the moment, M, along the arclength of the tube:

$$\theta_s = \int_0^1 \frac{M(l)}{EI} \, dl \tag{1}$$

During bending the cross-section of the tube will be distorted from a circle into an ellipse (ovalization), accompanied by the thickening and thinning of the wall thicknesses of the tube on the intrados and extrados, which are the inner surface contacting the die and the free outer surface. With the redistribution of the material, the centroid of the section moves toward the bend die, and the neutral axis moves along with it. Figure 1 shows the distortion of different cross-sections along the axis of a bent tube: the ovalization is zero at the two ends and reaches its maximum at the center of the bending area ($\psi = 0°$). The ovalization and thickness are exaggerated for clarity. As a result of the distortion, the moment of inertia will no longer be constant along the axis of the tube, but will be a function of the deformation which depends on the material properties, tube geometric parameters and bending parameters.

In previous springback predictions (Wang and Stelson, 1991), the moment of inertia of the tube after bending, I, is assumed to be 70 percent of the original moment of inertia, I_o, which is in agreement with the empirical result of Lukyanov and Zubkov (1968):

$$I = 0.7I_o \tag{2}$$

This rule-of-thumb is rough at best.

The objective of this paper is to find a relationship between the given axial curvature of a tube and the deformation of the cross-section of the tube during bending, from which a more accurate estimate of the moment of inertia can be obtained.

Process Description of Tube Bending

Rotary-draw bending machines are widely used for tube bending since they are versatile and generally more accurate than other kinds of bending machines. The tooling for rotary-draw bending is shown in Fig. 2. During bending, the clamp die holds the tube tightly against the bend die at the leading end of the tube. The bend die and clamp die rotate simultaneously while the pressure die moves together with the tube to provide a constraint and to reduce the friction between the surfaces of the tube and the pressure die. In this way the tube is forced to conform to the curvature of the surface of the bend die, which is circular.

When the bending moment is released, the material will tend to return to its original shape due to the elastic property of the material. This phenomena is called springback, and will create a slight increase in the radius of curvature of the bent tube and a reduction in the bend angle. Springback must be compensated for by overbending if an accurate bend angle is to be achieved.

Deformation Model of a Tube After Bending. The bending process of a tube can be simulated by the following mechanical model shown in Fig. 3: A tube is built-in to a circular foundation (the bend die) at its leading end and a bending moment, M, is exerted at its trailing end, which bends the tube gradually into contact with the bend die.

In the free body diagram of the tube, a bending moment, M, and concentrated loads, N_y and N_z, are exerted at one end and a bending moment, M', and concentrated loads, N_r and N_z' are exerted at the other end. A distributed contact force, q, is exerted on the intrados of the tube.

Previous Work. In the early part of this century, Bantlin (1910) found experimentally that a curved tube is much more flexible in bending than a straight tube of the same cross-section. Von Karman (1911) gave a theoretical explanation of this phenomenon. Since then, many studies have been conducted on the deformation of a tube after bending or related problems. Most of the studies focused on elastic deformation.

Von Karman studied the elastic deformation of a tube with a uniform wall thickness due to in-plane bending. The study shows that for a curved tube there is a tendency for the cross-section to flatten because of the continual change of the direction

---
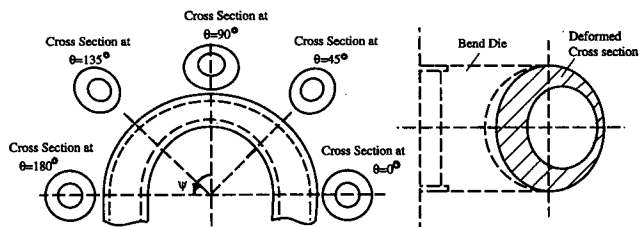
Fig. 1 The deformations at different cross-sections

Fig. 2 Tooling of a bending machine

of the stresses which are parallel to the center line of the tube and which balance the applied moment. The analysis is based on an application of the principle of minimum potential energy of the theory of elasticity in Rayleigh-Ritz fashion.

Brazier (1927) studied the ovalization of an infinitely long tube with a uniform wall thickness subjected to elastic pure bending. The solution of St. Venant's beam theory, which doesn't consider the distortion of the cross-section, plus an additional displacement was taken as an approximation of the true displacement when the effect of ovalization is taken into consideration. The additional displacements are determined by the condition that the strain energy of the tube will pass through a minimum. An approximate displacement field is assumed and the strain energy and its associated Euler equations are found.

Seddeik and Kennedy (1987) investigated the relation between the radius of a bend and the distortions of square hollow structural section members in the cold, pyramid roll-bending process. The variational principle of the total potential energy is adopted to predict this relationship. Quadratic terms are introduced in the strain-displacement relation to account for geometric nonlinearities. The total deformation theory is used as a constitutive relation. Zhang and Yu (1987) investigated the elastic-plastic cross-section deformation of an infinitely long tube in pure bending. The analysis is based on the energy principle. The variation of wall thickness is neglected. Since the tube is sufficiently long, the kinematic boundary condition does not enter the analysis. The total deformation theory is used as a constitutive relation.
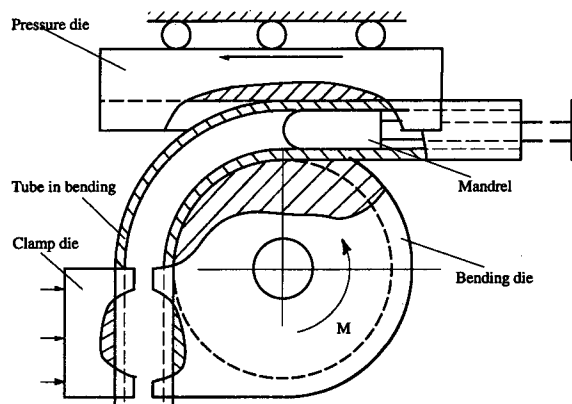
In the literature, no analysis considers a finite length tube and the variation of wall thickness. These effects become significant as the severity of bending increases. Since in manufacturing the above situation is frequently encountered, it is necessary to build a model to predict the deformation in this situation.

Coordinate System. The coordinate system used in the analysis is shown in Fig. 4, in which half of a tube that has been bent into a 180 deg. angle is shown. The cross-section of
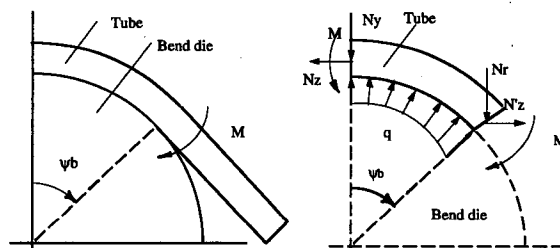

Fig. 3 Mechanical model and the free body diagram of a tube in bending

———— **Nomenclature** ————

A = area of the cross-section of a tube

D_{max}, D_{min} = lengths of the major and minor axes of the deformed tube cross section

E = Young's modulus

I_o, I = moment of inertia of the cross-section before and after bending

l = axial arclength of the tube

M = bending moment

N = axial load

n = exponential coefficient of the assumed axial curvature

q = contact force distribution between surfaces of the tube and bending die

r = distance between the tube origin and a point on the cross-section

R, D = radius and diameter of the tube

R_o = radius of curvature of the tube centerline

Rd = radius of curvature of the bending die

s = circumferential axis of the tube

S = moment of area of the cross-section of a tube

t = local coordinate along the thickness of the wall

T = tube wall thickness

x, y, z = Cartesian coordinates

u, v, w = components of the displacement field

U = strain energy

W = work done by external forces

α = dimensionless change of major axis: $\alpha = (D_{max} - D_o)/D_o * 100$ percent

β = dimensionless change of minor axis: $\beta = (D_o - D_{min})/D_o * 100$ percent

δ = dimensionless change of wall thickness

ϵ_s, ϵ_z, ϵ_r = strain components

ϵ_s^o, ϵ_z^o = strain components on the middle surface

ϵ = effective strain

φ = angular increment (see Fig. 4)

κ_z = axial curvature of the tube

λ = exponential coefficient of the displacement

ν = Poisson's ratio

Π = total potential energy

θ = circumferential angular coordinate

θ_s = spring back angle

ρ_s = circumferential radius of curvature of the tube

ρ_z = axial radius of curvature of the tube

σ_s, σ_z, σ_r = stress components

σ = effective stress

Ω = ovalization

ψ = angular coordinate along the tube

ψ_b = half of the bending angle

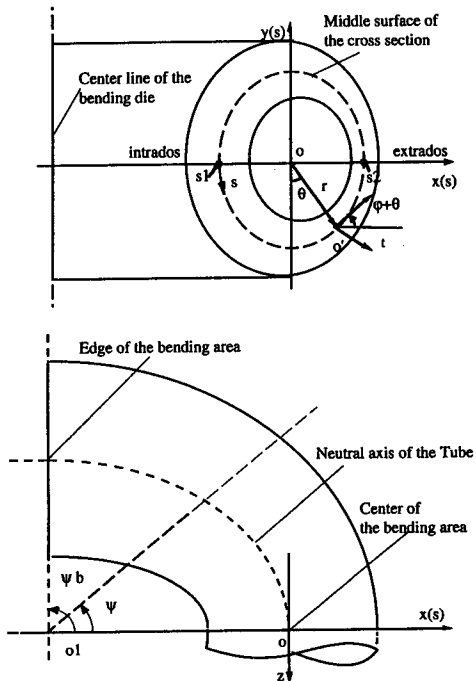ξ, ζ, η = coefficients of the displacement field

Fig. 4 Coordinate system

the tube is described by the Cartesian coordinates, $x(s)$, $y(s)$, where s is the circumferential arc length measured along the undeformed middle surface as shown in Fig. 5 and the coordinates, x, y and z, form a right-hand coordinate system. The middle surface is a cylinder which is located at the midpoint of the undeformed wall thickness. The origin of the t-axis, through which the wall thickness is measured, is located at the undeformed middle surface and the orientation of t is normal to the middle surface. The cross-section can also be described by a polar system (ρ, θ) which has its origin at o. 1 is the tube neutral axis which passes through point o, the origin of the $x(s)$, $y(s)$ coordinates. The axis of the bend die is normal to the x-z plane and passes through point o_1.

The center of the undeformed tube cross-section is located at point o and the distance between o and a point on the deformed middle surface is represented by r. φ is the increase in the angle between the tangent line which passes through point o' and the x axis due to cross-section distortion. This angle is zero when there is no cross-section distortion. The angle ψ, which measures the bending angle is measured from the center of the bending region.

The major assumptions used in the study are as follows:

- The plane which is perpendicular to the axis of the tube remains so after deformation;
- The material of the tube is incompressible and the elastic strains are neglected in the analysis. The effective stress and effective strain are related by a rigid, linear strain hardening material model;
- The deformation is symmetric with respect to both the x-z plane and the plane normal to x located at $\psi = 0$;
- The local unloading in the tube wall during bending is neglected and Ilyushin's simple loading theorem is satisfied;
- The friction forces between tooling and tube, and elongation of the neutral axis of the tube during bending are neglected.

Under the above assumptions, the physical model can be simplified further when the principle of minimum potential energy is used in the analysis. Since dies are regarded as rigid bodies and

there isn't any displacement along the direction of the distributed contact force, q, the work done by q is zero. Under the above assumption, the axial force, N, makes no contribution to the external work, W. As a result the displacement will be restricted to the plane that is perpendicular to the axis of the tube, i.e., the x-y plane.

On the other hand, although the contact force, q, and concentrated loads, N_x, N_y, will not appear in the expression for the external work, their contributions to the deformation are taken into consideration by prescribing a nonconstant axial curvature. This makes the problem different from a pure bending problem, in which the axial curvature is a constant along its axis.

Displacement Field. Based on the observation of experimental specimens, it is further assumed that the displacement has only a radial component. w is a function of three parameters, θ, ψ and t, which indicate the location that the displacement, w, represents.

Based on the observations of the experiment samples (refer to Fig. 5), the following function is chosen to approximate the pattern of the displacement:

$$w(\theta, \psi, t) = R\xi' \cos 2\theta + R\zeta' \sin 3\theta - t\eta' \sin \theta$$

$$-T/2 < t < T/2, \quad 0 < \psi < \psi_b, \quad 0 \le \theta \le 2\pi \quad (3)$$

It is found that the above function can well represent the deformation of the cross-section if the three coefficients, ξ' ζ' and η', are properly chosen. Along the axis of the tube, it is prescribed that the axial curvature, κ_z, varies proportionally to the term $(\cos^n \psi)$:

$$\kappa_z = 1/\rho_z = \cos^n(\pi\psi/2\psi_b)/R_d \quad (4)$$

where the coefficient n is obtained from the experiment specimens. It is found that when $n = 0.7$, Eq. (4) can best reflect the change of the axial curvature of the tube after bending. When $n = 0$, the displacement field degenerates into the pure bending case.

The coefficients of the displacement function, ξ', ζ' and η', are assumed to vary proportionally to the term $(\cos^n\psi)$ also, or:

$$\xi' = \xi \cos^n (\pi\psi/2\psi_b)$$
$$\zeta' = \zeta \cos^n (\pi\psi/2\psi_b)$$
$$\eta' = \eta \cos^n (\pi\psi/2\psi_b) \quad (5)$$

Thus, the assumed displacement function becomes:

$$w(\theta, \psi, t) = R\xi \cos^n (\pi\psi/2\psi_b) \cos 2\theta$$
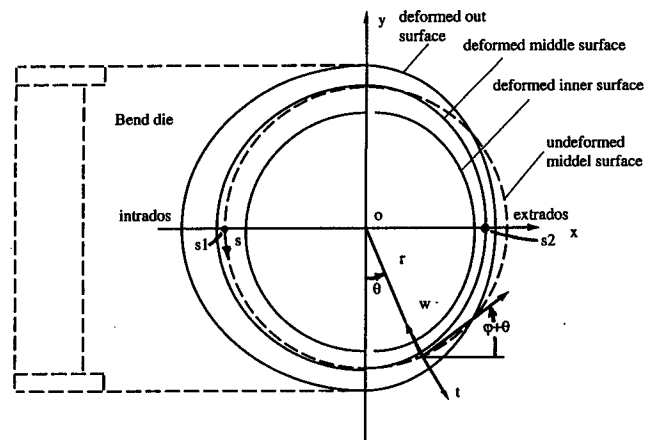$$+ R\zeta \cos^n (\pi\psi/2\psi_b) \sin 3\theta - t\eta \cos^n (\pi\psi/2\psi_b) \sin \theta \quad (6)$$

Fig. 5 Cross-section deformation pattern

where the constants, ξ, ζ and η, will be determined by the principle of minimum potential work.

In the assumed displacement function (3), the contribution of each term can be shown clearly in the polar system (ρ, θ). A point located at (ρ, θ) on a cross-section moves to $(\rho + w, \theta)$ after deformation. The term $(R\xi' \cos 2\theta)$ will change the cross-section from a circle into an ellipse which is symmetric to both x and y axis. After superposition of the term $(R\zeta' \sin 3\theta)$, a nonsymmetric cross-section with respect to y axis is formed. The term $(\eta't \sin \theta)$ will give a wall thickness thicker at the intrados and thinner at the extrados and the negative sign comes from the defined orientation of w, which is the opposite of that of the t axis. At the two edges of the bending area where $\psi = \pm\psi_b$, we have:

$$\cos^n (\pi\psi/2\psi_b) = 0 \quad \text{or} \quad \xi' = \zeta' = \eta' = 0 \quad \text{and} \quad \kappa_z = 0$$

while at the middle of that bending area where $\psi = 0°$:

$$\cos^n (\pi\psi/2\psi_b) = 1 \quad \text{or} \quad \xi = \xi', \zeta = \zeta', \eta = \eta'$$

$$\text{and} \quad \kappa_z = (1/R_d)$$

which agrees with what is observed in experiments. Thus, the pattern of the displacement field chosen is expected to agree with what is found in the experiment while the magnitude of the displacement will be determined by the principle of minimum potential work.

From Eqs. (3, 4), the distance between the center of undeformed cross-section, o and a point at deformed middle surface, o' (where $t = 0$) is:

$$r(\theta, \psi) = R[1 + \xi \cos^n (\pi\psi/2\psi_b) \cos 2\theta$$

$$+ \zeta \cos^n (\pi\psi/2\psi_b) \sin 3\theta] \quad (7)$$

This distance is R before the tube is bent.

Geometric Relations and Strain Field. As shown in Fig. 5, consider a small segment of tube with a length of dz, along which the ovalization can be regarded as uniform. On the middle surface, the relation between a small segment of circumferential arc length, ds, and its projections on x and y axis, dx and dy, leads to the geometric relation:

$$\frac{dx}{ds} = (1 + \epsilon_s^o) \cos (\varphi + \theta)$$

$$\frac{dy}{ds} = (1 + \epsilon_s^o) \sin (\varphi + \theta) \quad (8)$$

where ϵ_s^o is the circumferential strain on the middle surface.

After bending the circumferential radius of curvature, ρ_s, of the middle surface can be found through a differential geometry formula:

$$\rho_s = \left| \left[\left(\frac{dy}{ds}\right)^2 + \left(\frac{dx}{ds}\right)^2 \right]^{3/2} \middle/ \left[\left(\frac{d^2y}{ds^2}\right)\left(\frac{dy}{ds}\right) \right.\right.$$

$$\left.\left. - \left(\frac{dx}{ds}\right)\left(\frac{dx^2}{ds^2}\right) \right] \right| \quad (9)$$

This circumferential radius of curvature was R before bending.

From (8) and (9), we have:

$$\rho_s = \left| (1 + \epsilon_s^o) \middle/ \left(\frac{d\varphi}{ds} + \frac{d\theta}{ds}\right) \right| \quad (10)$$

$$\frac{d\varphi}{ds} = \left| (1 + \epsilon_s^o)\left[r^2 + 2\left(\frac{dr}{d\theta}\right)^2 - r\frac{d^2r}{d\theta^2} \right] \right| \quad (11)$$

On the other hand, in the polar system (ρ, θ) the circumferen-
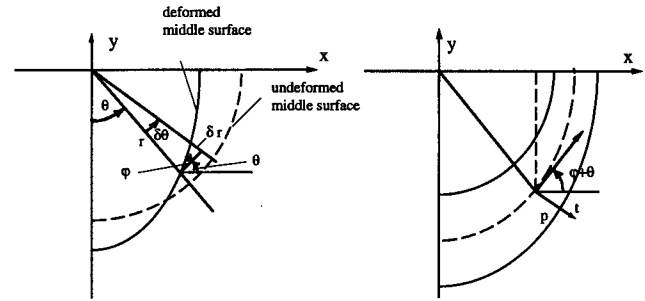
Fig. 6   Middle surface before and after deformation

tial radius of curvature on middle surface, ρ_s, can be expressed as:

$$\rho_s = \left| \left[r^2 + \left(\frac{dr}{d\theta}\right)^2 \right]^{3/2} \middle/ \left[r^2 + 2\left(\frac{dr}{d\theta}\right)^2 - r\frac{d^2r}{d\theta^2} \right] \right| \quad (12)$$

Physically the term $(d\varphi/ds)$ is the change of radius of curvature on the middle surface after deformation.

From the above relations, the strain field can be determined:

$$\epsilon_z = [x + t \sin (\theta + \varphi)]/\rho_z = \epsilon_s^o + t \sin (\theta + \varphi)/\rho_z \quad (13)$$

where ϵ_s^o is the axial strain on the middle surface. The term sin $(\theta + \varphi)$ can be found through the relation of a circumferential arc length at the middle surface before and after bending as shown in Fig. 6:

$$\sin (\theta + \varphi) = \sin \theta \cos \varphi + \cos \theta \sin \varphi$$

$$= (r \sin \theta + r_\theta' \cos \theta)/(r^2 + r_\theta'^2)^{1/2}$$

The circumferential strain can be determined as follows (Fig. 7). On a cross-section consider an undeformed circumferential fiber with a length dl located at (θ, t):

$$dl = \left(\frac{ds}{d\theta} + t\right)d\theta = \left(1 + \frac{d\theta}{ds}\right)ds \quad (14)$$

After deformation the fiber length becomes dl^*:

$$dl^* = (1 + \epsilon_s^o)ds\left(1 + \frac{t}{\rho_s}\right) \quad (15)$$

where ρ_s is the circumferential radius of curvature of the tube. The circumferential strain can be found from Eq. (14) and Eq. (15):

$$\epsilon_s(\theta, t) = \frac{dl^* - dl}{dl} = \left(\epsilon_s + t\frac{d\theta}{ds}\right) \middle/ \left(1 + \frac{d\theta}{ds}\right)$$

$$= \frac{t}{R + t}\left(\epsilon_s^o + t\frac{d\varphi}{ds}\right) \quad (16)$$

If we consider the bending component of ϵ_s only, there will be no elongation along the circumferential direction on the middle surface of the tube, or:

$$\epsilon_s^o = 0$$

Stress Field. From the total deformation theory the relations between the strain and stress fields are:

$$s_{ij} = \frac{2}{3}\frac{\bar{\sigma}}{\bar{\epsilon}} e_{ij}$$

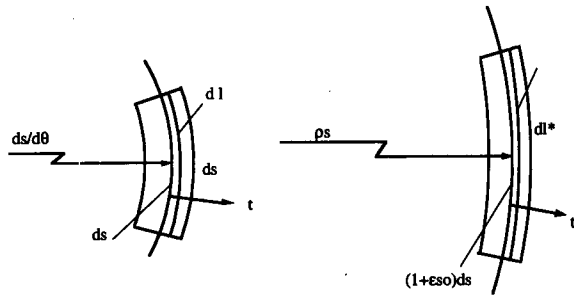$$\epsilon_{kk} = \frac{1 - 2\nu}{E} \sigma_{kk} \quad (17)$$

Fig. 7 Circumferential arc before and after bending

where σ_{ij}, e_{ij} are deviatoric stress and strain tensors:

$$s_{ij} = \sigma_{ij} - \tfrac{1}{3}\sigma_{kk}\delta_{ij}$$

$$e_{ij} = \epsilon_{ij} - \tfrac{1}{3}\epsilon_{kk}\delta_{ij} \tag{18}$$

and $\bar{\sigma}$ and $\bar{\epsilon}$ are effective stress and strain, respectively. The effective strain is found through the Prantl's theory:

$$\bar{\epsilon} = \tfrac{2}{3}[\epsilon_s^2 + \epsilon_z^2 + \epsilon_r^2 - \epsilon_s\epsilon_z - \epsilon_r\epsilon_s - \epsilon_z\epsilon_r]^{1/2} \tag{19}$$

The material behavior is described by rigid linear work hardening:

$$\bar{\sigma} = \sigma_0 + \sigma_1\bar{\epsilon} \tag{20}$$

where σ_0 and σ_1 are the material yield stress and strain hardening coefficient, respectively. The tension and compression tests show that the tubes have different flow stress behavior in tension and compression. This effect is included in the model.

From Eqs. (18)–(20), the stress tensor can be expressed as:

$$\sigma_{ij} = \frac{2}{3}\frac{\bar{\sigma}}{\bar{\epsilon}}\epsilon_{ij} - \frac{2}{9}\frac{\bar{\sigma}}{\bar{\epsilon}}\epsilon_{kk}\delta_{ij} + \frac{1}{3}\frac{E}{1-2\nu}\epsilon_{kk}\delta_{ij} \tag{21}$$

Assuming that the shear stresses are negligible, and that the elastic part of the strains is negligible (no volume change after deformation):

$$\epsilon_s + \epsilon_z + \epsilon_r \cong 0 \tag{22}$$

Substituting Eq. (22) into (21) gives:

$$\sigma_z = \frac{2}{3}\frac{\sigma_0 + \sigma_1\bar{\epsilon}}{\bar{\epsilon}}\epsilon_z$$

$$\sigma_s = \frac{2}{3}\frac{\sigma_0 + \sigma_1\bar{\epsilon}}{\bar{\epsilon}}\epsilon_s$$

$$\sigma_r = \frac{2}{3}\frac{\sigma_0 + \sigma_1\bar{\epsilon}}{\bar{\epsilon}}(-\epsilon_z - \epsilon_s)$$

$$\bar{\epsilon} = 2\sqrt{(\epsilon_z^2 + \epsilon_s^2 + \epsilon_z\epsilon_s)/3} \tag{23}$$

Potential Energy. By definition the total potential energy, Π, is the difference between the strain energy in the tube, U, and the work done by the external forces, W.

$$\Pi = U - W \tag{24}$$

The strain energy can be found by an integration over the volume of the deformed body:

$$U = 4\int_0^{\psi_b}\int_{s_1}^{s_2}\int_{-T/2}^{T/2}\left(\int_0^{\sigma_z}\sigma_z d\epsilon_z + \int_0^{\sigma_s}\sigma_s d\epsilon_s\right.$$

$$\left. + \int_0^{\epsilon_r}\sigma_r d\epsilon_r\right)d\psi dsdt \tag{25}$$

where the integration is performed on a quarter of the volume due to the symmetry of the problem. The limits, S_1 and S_2, indicate the intrados and extrados of the tube.

The only external force which does work to the system is the bending moment, M. The external work done by the moment is:

$$W = 2M\psi_b \tag{26}$$

Thus, the total potential energy is found to be:

$$\Pi = 4\int_0^{\psi}\int_{s_1}^{s_2}\int_{-T/2}^{T/2}\left(\int_0^{\sigma_z}\sigma_z d\epsilon_z + \int_0^{\sigma_s}\sigma_s d\epsilon_s + \int_0^{\epsilon_r}\sigma_r d\epsilon_r\right)$$

$$\times \sqrt{r^2 + \left(\frac{d^2r}{d\theta^2}\right)^2}\,d\psi dsdt - 2M\psi_b \tag{27}$$

Boundary Conditions. The boundary conditions for displacement have been implied by the prescription of the axial curvature of the tube:

$$\kappa_z = 1/\rho_z = 1/R_d \quad \psi = 0°$$

$$\xi' = \zeta' = \eta' = 0 \quad \psi = \psi_b \tag{28}$$

The static boundary conditions insure that the external bending moments equal the internal moment at the two ends of the bending region:

$$M_o = M_i$$

Since a rigid linear work hardening model is used the internal moment will be:

$$M_i = \sigma_o S = \sigma_o \int_A x dA \tag{29}$$

Comparison of Numerical and Experimental Results

Numerical Solution. The numerical solution is found through a minimization approach. The problem is a nonlinear programming problem subject to a set of constraints. A polyhedron search algorithm with a flexible tolerance method is used to solve the problem (Himmelblau, 1972). To increase the efficiency of the approach, the algorithm improves the value of the objective function by using the information provided by the points which do not satisfy the constraints during the search
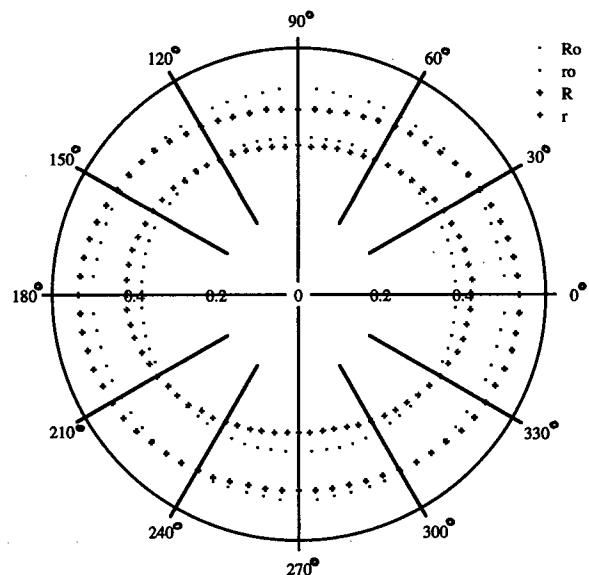

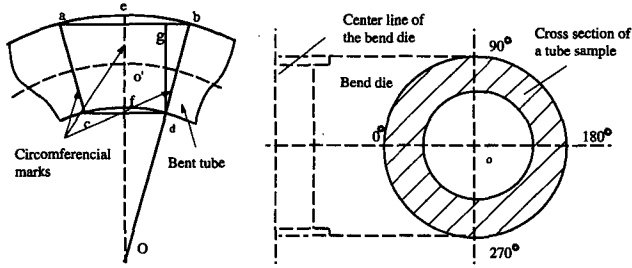**Fig. 8 Ovalization at the center of the bending region**

Fig. 9 The position of a tube on the bend die

Fig. 11 Ovalization on different cross-sections

process. The algorithm also ensures that the constraints are satisfied when the solution is reached.

The numerical calculation is made on an example of aluminum tube. The geometrical parameters are:

$$D_o = 25.40 \text{ mm} \quad D_i = 19.56 \text{ mm}$$
$$T = 2.92 \text{ mm} \quad R_d = 50.80 \text{ mm}$$

Three coefficients in the displacement function are obtained through a minimization. The values of the coefficients for the given radius of the bend die are:

$$\xi = 0.081 \quad \eta = 0.112 \quad \zeta = 0.0031$$

In the calculation, 10 elements are taken along the axis of the tube. In each element the axial curvature is taken as a constant, which equals the curvature at its center. The deformation of the cross-sections on two sides of each element are evaluated. Half of the elements are actually used in the numerical computation due to the symmetry of the problem.

After the displacement field is found, the ovalization on different cross-sections and the changes of the wall thicknesses of the tube at different cross-sections and different circumferential positions are calculated and summarized in Fig. 8, Fig. 11 and Fig. 12. In Fig. 8, the dotted lines represent the inner and outer surfaces of the tube before bending; the crossed lines represent the inner and outer surface of the tube after bending.

The results are checked by evaluating the potential energy in the neighborhood of the minimum. It is found that there is no other minimum inside the neighborhood which represents a reasonable displacement field.

In the present analysis all integrations were performed on the undeformed configuration, instead of the deformed configuration as it should be. The same approximation was also used by Seddeik and Kennedy (1987) and Zhang and Yu (1987) since much less computation is required. On the other hand, this will unavoidably introduce some error into the numerical results.

After the displacement field is obtained, the moment of inertia of the cross-section with respect to y axis can be found through an area integration:

$$I(y) = \int_A [R + w(\psi, \theta, t) \sin \theta]^2 dA \qquad (30)$$

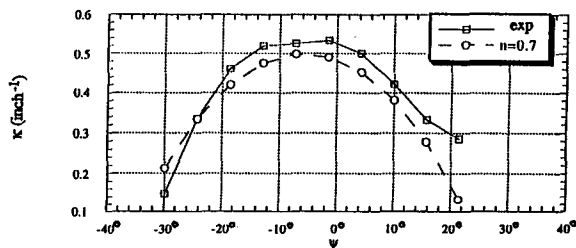where $w(\psi, \theta, t)$ is the displacement determined by the minimization.
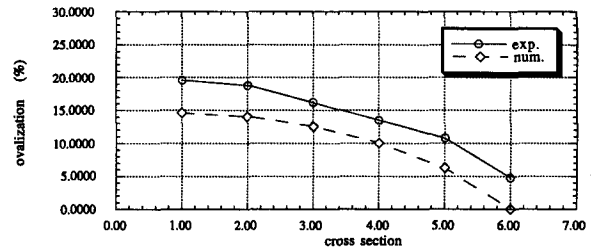
Experimental Results. The bending tests were performed on a rotary draw tube bender (Teledyne Pines Co.). An angular encoder was attached to the axis of the bending die to monitor the bending angle. The machine was operated manually while the bending angle can be read out from the screen of a computer which collected data from the encoder. The sample tube had the same geometry as that used in the numerical analysis. The tube was bent into a 60 deg. angle. The bend die has a circular shape with a radius of 50.8 mm (2 in).

Before bending the surface of a tube is clearly marked with an orthogonal grid pattern consisting of rings spaced every 5.08 mm (0.2 in.) along the axis and axial lines spaced every 30 deg. around the circumference. The radius of curvature along the axis of the tube can be approximately found from the following measurements (Fig. 9):

$$\rho_z = \overline{oo'} = \frac{\overline{dg}}{\overline{cd}} \left[\overline{bd}^2 - \frac{1}{4}(\overline{ab}^2 - \overline{cd}^2) \right]^{1/2} - \frac{1}{2} \overline{ef} \qquad (31)$$

where the length of the segments $\overline{ab}$, $\overline{cd}$, $\overline{bd}$, $\overline{dg}$ and $\overline{ef}$ can be measured directly.

From the measurements, the variation of the wall thickness and the ovalization can be calculated. The variation of the axial curvature is shown in Fig. 10 in which experimental data are compared with their theoretical approximation, which is used in theoretical analysis:

$$\kappa_z = 1/\rho_z = \cos^n (\pi \psi / 2 \psi_b)/R_d$$

Comparison of Numerical and Experimental Results. A comparison of analytical and experimental results were made using the following quantities:

(i)   ovalization: $\Omega = (D_{max} - D_{min})/D_o * 100\%$;
(ii) dimensionless change of wall thickness: $\delta = (t - T)/T * 100\%$
(iii) moment of inertia: $I = I(y)$

where D_{max}, D_{min} are the major and minor axes of the deformed tube respectively; D_o is the original outside diameter; T and t are the original and deformed wall thicknesses. Figure 11 and Fig. 12 summarize the results of the comparisons.

After the three constants, ξ, η and ζ, in the expression for the displacement function are determined, the moment inertia of the cross-section with respect to the y axis at the middle of the bending region can be calculated using Eq. (4):

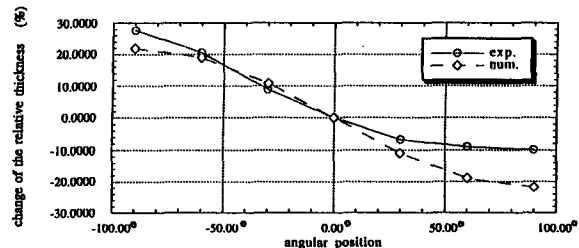Fig. 10 Axial curvature of the sample and its approximation

Fig. 12 Comparison of dimensionless change of wall thickness

$$I_o = 0.0321 \text{ in}^4 \quad I_e = 0.0288 \text{ in}^4 \quad I_c = 0.0278 \text{ in}^4$$

$$(I_o - I_e)/I_o = 0.1028 \quad (I_o - I_c)/I_o = 0.1340$$

$$(I_e - I_c)/I_e = 0.0347$$

where I_o is the moment of inertia of the original cross-section and I_e, I_c are the moments of inertia of the deformed cross-sections from experiment and computation, respectively.

Discussion on the Comparison. The theoretical results give displacement fields which are almost symmetric to both x and y axes as a result of the underprediction of the parameter, ζ, in the displacement function. The over simplification of the interaction between tube and bend die may be responsible for the underprediction. For ovalization, the theory gives an underprediction of about 25 percent at the center of the bend. For the change of the wall thickness, the theory also gives a 25 percent underprediction.

Although 25 percent differences on average are found in the ovalization at the center and the change of wall thickness, only about a 2 percent difference is found in the moment of inertia in spite of the fact that the moment of inertia depends on the fourth power of the cross-section dimensions.

In the present analysis, the deformation is calculated from the given axial curvature of the deformed tube and the actual axial curvature is approximated by Eq. (4). Figure 10 shows that the predicted axial curvature is always smaller than that of the experimental data. As a result, the deformation predicted by the approximated axial curvature will be smaller than the actual deformation.

Another possible source of error is the assumption of (5). Although the function

$$\kappa_z = 1/\rho_z = \cos^{0.7}(\pi\psi/2\psi_b)/R_d$$

can approximate the change of the axial curvature well, it is not necessarily true that the parameter ξ, ζ and η, will change along the axial direction in the same way. In the present theory, the purpose of the above assumption is to reduce the amount of the numerical computation by searching over three rather than four variables for minimizing the energy.

Conclusions and Suggestions for Future Work

The final goal of the study, to improve the precision of a real-time controlled tube bending system, requires an accurate prediction of the deformation of a tube cross-section after bending. A theoretical and experimental investigation of the bending of a tube in the plastic region has been undertaken. It has been shown that the results of the present theory are reasonable. The present theory gives a prediction of the ovalization and the wall thickness change which has not been found in previous work.

The theory could also provide the basis for a real-time control strategy where the unknown parameters in the approximate model are estimated based on measurements taken from the process. Candidate measurements include forces and displacements taken from the current or previous bend and springback from the previous bend.

The contribution of the present study is that it provides a theoretical basis to predict the deformation after bending. At the same time, the theory may form a good starting point to give a better prediction with some modifications in the future.

After analyzing the results from the present study, it is suggested that in order to achieve a better theoretical prediction, the following work might be done:

(i) More accurate boundary conditions may be prescribed. For the rotary-draw bending process, it is suitable to find the cross-sectional deformation from the assumed axial curvature since we know the shape of the bend die and we know how the tube will follow the shape of the die. On the other hand, the experimental results show that the tube does not follow the shape of the die completely and the proposed boundary condition (28) is too simple to reflect the actual case completely.

At edges of the bending region, the curvature of the bend die changes from a constant to zero. The deformation would not stop at the edges suddenly due to the continuity of the material. Thus, the boundary conditions at the two edges should also be reconsidered.

(ii) The interaction between the bend die and the tube should be taken into consideration. The half circle slot on the bend die provides a constraint on the deformation.

(iii) The assumption, Eq. (5), that the deformation will vary proportionally to the term

$$\cos^{0.7}(\pi\psi/2\psi_b)$$

should be eliminated although it will increase the computation time significantly. Instead of using a constant 0.7, a fourth parameter, n, should be added into the assumed displacement field and its value should be determined in the process of minimization.

(iv) The axial load might be taken into consideration. The axial load is provided by the friction force between clamp die and tube and is balanced by the contact distributed force between bend die and tube.

References

Bantlin, A., 1910, "Formanderung und Beanspruchung federnder Ausgleichsrohren," *Zeitshrifts VDI*, Vol. 54, pp. 43–49.

Brazier, L. G., 1927, "On Flexure of Thin Cylindrical Shells and Other Thin Sections," *Proc. R. Soc. London., Ser. A*, Vol. 116, pp. 104–114.

Himmelblau, D. M., 1972, *Applied Non-linear Programming*, McGraw-Hill, N.Y.

Karman, Th. v., 1911, "Uber die Formanderung Dunnwandiger Rohre, insbesondere federnder Ausgleichsrohre," *Z. Ver. deit. Ing.*, Vol. 55, pp. 1889–1895.

Lukyanov, V. P., and Zubkov, A. I., 1968, "Investigation of Tube Bending on a Tube Bending Machine with Mandrel," *UDC 621.774.63.06, Translated from Khimicheskoe i Neftyanoe Machinostroenie*, Vol. 11, pp. 22–23.

Seddeik, M. M., and Kennedy, J. B., 1987, "Deformations in Hollow Structural Section (HSS) Members Subjected to Cold-bending," *Int. J. Mech. Sci.*, Vol. 29, pp. 195–212.

Wang, W. C., and Stelson, K. A., 1991, "Computer Aided Manufacturing for Three-dimensional Tube Bending with On-line Springback Compensation," *Tran. North Am. Manu. Res. Ins. SME*, pp. 70–76.

Zhang, L. C., and Yu, T. X., 1987, "An Investigation of the Brazier Effect of a Cylindrical Tube under Pure Elastic-plastic Bending," *Int. J Pres. Ves. & Piping*, Vol. 30, pp. 77–86.